CRITICAL REVIEW OF CHALLENGES AND POTENTIALS FOR SNOW DRIFT SIMULATION

Arnulf Wurzer[1,*], Arnold Studeregger[1], Peter Fischer[2]
[1]Zentralanstalt fuer Meteorologie und Geodynamik, Klusemannstrasse 21, 8053 Graz, AUSTRIA
[2]dTech Steyr - Dynamics and Technology Services GmbH, Steyrerweg 2, A - 4400 Steyr, AUSTRIA

ABSTRACT: A review of current snow drift models is given. Further a turbulent snow drift model based on an Algebraic Slip Model approach is validated. The driving wind field is computed by extracting time dependent boundary conditions from Numerical Weather Prediction by a mass conserving optimization approach. The results are compared to observations at the Planneralm, Austria. The influence of different snow parameters is investigated and it's concluded, that the snow particle transport is more sensitive to the wind speed, than to various snow property parameters of classical models.

KEYWORDS: Optimization, Algebraic Slip Model, Aerodynamic entrainment, snow drift, CFD, time dependent boundary conditions

1 INTRODUCTION

Snow avalanches are mostly triggered by a critical snow depth. The highest snow depths are generally accumulated in leeward slopes, chutes, and dingles, mainly caused by wind and snow drift. Therefore a snow drift simulation in mountain regions is an important base for avalanche warning services.

Worldwide, there are considerable efforts to simulate snow drift by wind. In this work a critical review of potentials and challenges for snow drift simulation models is given. Finally a turbulent snow drift model, including time dependent boundary conditions (BCs) from Numerical Weather Prediction (NWP) model, based on the work of Schneiderbauer and Pirker (2010, 2011), is applied and validated. The results are compared to measurements from weather stations on the Planneralm. The positions of the weather stations and characteristic avalanches of this area are shown in Figure 1. At these stations wind speed, wind direction, air temperature, snow depths, solar irradiation and air moisture is measured. Additionally, webcams took pictures of snow poles and the whole moun-

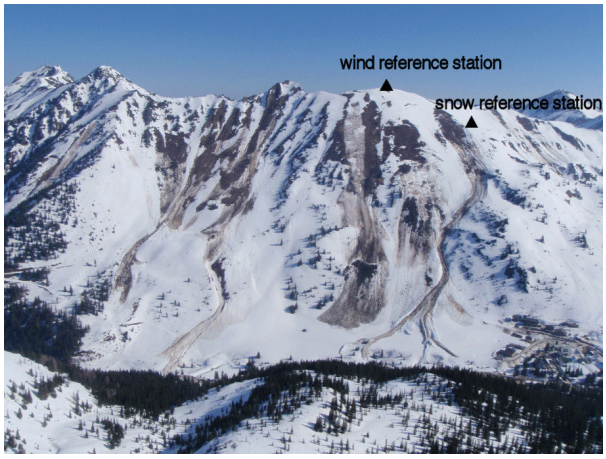

Figure 1: Measurement site at the Planneralm (source: Avalanche Service Styria)

*Corresponding author address: Arnulf Wurzer, Zentralanstalt fuer Meteorologie und Geodynamik (ZAMG), Klusemannstrasse 21, 8053 Graz, AUSTRIA; Tel. +43 0316 24 200; email: arnulf.wurzer@gmx.at

tain side for a qualitative comparison of the snow distribution.

2 REVIEW OF SNOW DRIFT MODELS

2.1 State of the art

The work of (Bagnold, 1941) introduced the foundation for our current understanding of aeolian snow and sand transport. In the 90's further studies by Anderson and Haff (1991) and Pomeroy and Gray (1990) yield to a more formalized classification of wind induced particle transport and a deeper understanding of the saltation transport mode.

Liston et al. (2007) presented an enhancement of the three-dimensional (3-D) transport model SnowTran-3D, which is based on the simulation of snow-transport processes in variable topography and different snow climates. The saltation mode is based on the semi-empirical formulae of Pomeroy and Gray (1990). In addition, SnowTran-3D has been coupled to a high-resolution, spatially distributed meteorological model (MicroMet) to provide more realistic atmospheric forcing data.

A transient 3-D snow drift model was introduced by Gauer (1999), in which the turbulent suspension is modeled by an incompressible fluid (air) and determined by computational fluid dynamics (CFD). The saltation transport mode is computed separately by typical grain trajectories, which included ejection of grains due to impacts of other snow particles. Precipitation is also included into this model. Based on this two-way coupling snow drift model, Lehning et al. (2000) combined the snow cover model SNOWPACK and proposed an snow drift index based on SNOWPACK model calculations.

Doorschot and Lehning (2002) considered a simplified deformation of the wind field within the saltation layer, but still no turbulence effect is taken into account.

Many others made important efforts in the field of snow drift simulation (e.g. Naaim-Bouvet et al., 2004). In the models discussed above, snow drift of particles in suspension are considered as a continuum. Within the saltation layer mass fluxes are specified by typical particle trajectories (cf. Gauer, 1999; Doorschot and Lehning, 2002). But computing all particle trajectories within a Lagrangian frame would lead to an enormous computational effort.

Smaller-scale deposition patterns such as dunes and cornices can only be computed by high resolution simulations. Mott and Lehning (2009) investigated the effect of the wind field resolution and obtained most realistic wind field and deposition patterns with the highest resolution of 5 m by applying the meteorological model ARPS to compute the mean wind field. Snow deposition is computed by the transport module Alpine3D (cf. Lehning et al., 2006).

To conclude, several main areas are identified which appear most critical for achieving improved results in snow drift simulations. Important areas are:

- Application of high-resolution local wind fields, including transient behaviour.
- Ground surface modeling and the ability to change the surface shape during erosion / deposition events.
- Assessment of turbulence effects in the air flow.
- Erosion and deposition behaviour of snow with respect to numerous physical properties like temperature, grain size, wind speed, gross density and erosion rate.

2.2 Snow drift model

It's common to distinguish between three different types of snow transport: the creeping or reptation zone, the saltation zone and the suspension zone (cf. Anderson and Haff, 1991; Bagnold, 1941). Snow transport occurs if the friction velocity $u_\star$ exceeds a certain threshold, which was first defined by Bagnold as

$$u_{\star t} = A\sqrt{\frac{\rho_p - \rho_a}{\rho_a} g d}, \quad (1)$$

where ρ_P is the density of the particle, ρ_a the density of air and d the grain diameter. Schmidt (1980) suggested a formulation of $u_{\star t}$ for snow, which included also the snow bulk properties, microstructure and cohesive force. He cited a relation between T (in °C) and F_C normalized to F_C at -15 °C as

$$\frac{F_C(T)}{F_{C(-15\ ^\circ C)}} = 8 \exp\left(0.141\ T\right). \quad (2)$$

His estimation of the treshold wind speed for a plane is used to calculate the treshold shear stress τ_t (using the relation $u_\star = \sqrt{\tau/\rho_a}$):

$$\tau_t = \frac{\eta}{\Gamma} \frac{\left(0.666\left(\rho_P - \rho_{air}\right) g d_P + F_C/A\right) \tan\beta'}{1 + 0.85 \tan\beta'}. \quad (3)$$

β is the angle of repose and assumed to be 33° and β' the mean drag level, which is approximately 24°. Estimating the mean critical shear stress, Schmidt (1980) implies the constant $\eta = 0.21$ describing the packing ratio and $\Gamma = 2.5$ representing the ratio of the maximum to the mean turbulent impulse. Assuming that the drag force executes on the cross-section $A = \pi d_P^2/4$, we discount F_C divided by the cross-section.

There are only a few studies which focus their attention on the aerodynamic entrainment. For example Anderson and Haff (1991) and Williams et al. (1990) proposed the interception of grain transport by wind as a linear relationship between the entrained grains per unit area (N_{ae}) and the exerted shear stress

$$\frac{\partial N_{ae}}{\partial t} = \xi_{ae}\left(\tau(z=0) - \tau_t\right). \quad (4)$$

The coefficient ξ_{ae} is in many models defined as a constant coefficient. For example in Anderson and Haff (1991) ξ_{ae} is taken as $10^5\ \mathrm{N^{-1}s^{-1}}$ for sand particles. This value was also used in many snowdrift models, e. g. Gauer (1999) or Doorschot and Lehning (2002). Shao and Li (1999) suggested ξ_{ae} some magnitudes greater and estimated the entrainment value for quartz particle with a diameter of $350\ \mu\mathrm{m}$ to be $\xi_{ae} = 5 \times 10^7\ \mathrm{N^{-1}s^{-1}}$. For smaller particle the value should be even larger.

Zones of deposition can be either determined by Bagnold's (1941) 'stick-slip' criteria or by using a expression for the rebound probability of snow particles proposed by Anderson and Haff (1991) and used in the model of Andreotti (2004) as followed:

$$P_R(v_i) = 0.05 + 0.95 \exp\left(-\frac{v_i}{j\sqrt{dg}}\right). \quad (5)$$

v_i is the impact velocity of the particles and j an impact parameter set to 10.

3 ADVANCED SIMULATION BY ALGEBRAIC SLIP MODEL AND EXTRACTING TIME DEPENDENT BC'S

In the current work a fully turbulent, non stationary simulation approach based on the work of Schneiderbauer et al. (2008) is used. The main differences to other models are a multiphase Algebraic Slip Model for the snow drift and time dependent BC's for the wind field, obtained by NWP models. The snow particles in saltation and suspension are accounted as a continuous phase and therefore no separately numerical domains as in many other models (e.g. Gauer, 1999; Liston et al., 2007; Doorschot and Lehning, 2002) are computed. The model is fully turbulent and therefore the whole snow transport and the computation of the shear stresses is affected by turbulence. Accounting the coupling of wind flow to a deforming snow cover, the geometry is modeled dynamically. For further information and the enclosure of turbulent effects, the reader is referred to Schneiderbauer et al. (2008).

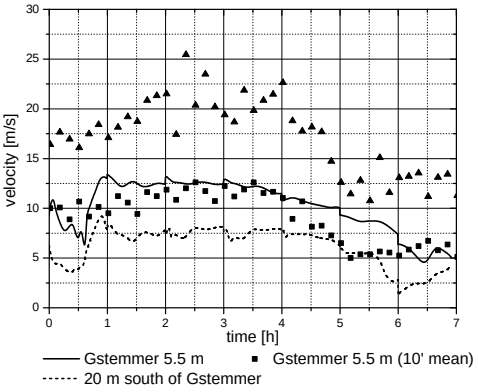

Figure 2: Comparison of the measured (symbols) and computed (lines) wind speed at the Gstemmer peak. Simulation starts at 06^{00} CET.

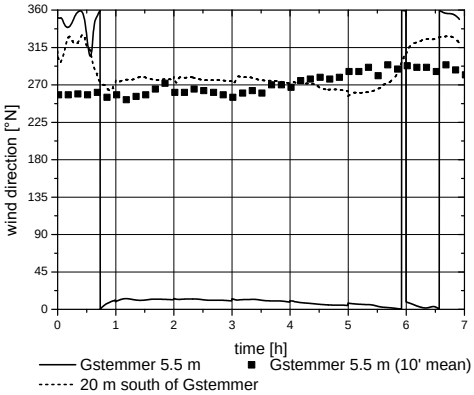

Figure 3: Comparison of the measured (symbols) and computed (lines) wind direction at the Gstemmer peak. Simulation starts at 06^{00} CET.

3.1 Analysis of the snow drift at the Planneralm

The Flow over the Planneralm is computed by extracting the time dependent BCs from the NWP model ALADIN-Austria (e.g. Wang et al., 2006) by a Mass Conserving Optimization approach proposed by Schneiderbauer and Pirker (2010, 2011) . Further the commercial flow solver FLUENT is used to solve the Navier-Stokes Equations.

The unsteady wind field at the Planneralm is computed based on an hourly ALADIN-Austria forecast, which starts at Wednesday the 3^{rd} of March 2010, at 06^{00} CET (Central European Time). The model results are compared to the measured wind speed and wind direction at the wind reference station, which is on top of the Gstemmer peak. The snow deposition patterns computed by the described snow drift model are validated by snow poles and measured data at a snow reference station at the south slope of the Gstemmer peak. In Figure 1 and 9 the locations of the reference stations are displayed.

From $t = 1$ h on, the wind speed is in satisfactorily agreement with the measured values at the reference station (cf. Figure 2). In Figure 3 the wind direction at the reference station differs from the measurements considerably. This deviation is probably due to a coarse grid interval of 25 m (cf. Section 3.2), which causes a rather rounded peak of the numerical grid compared to reality. But as you can see in Figure 3, the wind direction 20 m south of the reference station is in good agreement with the measurement. At westerly winds the stream is redirected throughout the valley placed on the north side of the Gstemmer peak. Due to this canalization effect the west wind strikes the redirected wind from the north at the Gstemmer crest. This effect is shown on the computed wind vectors at Figure 9.

3.2 Numerical grid

For the numerical analysis of the flow over the Planneralm a hexahedral finite volume mesh is used. The horizontal extensions of the grid are 7.8 km in west-east and north-south direction, which is slightly smaller than the ALADIN-Austria grid resolution of 9.6 km. The top boundary is placed 2.5 km above the Gstemmer peak. The horizontal resolution is 10 m around the wind reference station on top of the Gstemmer peak, which is linearly expanded towards the boundaries. The heights of the vertices at the surface level are bilinearly interpolated from a 25 m resolved digital elevation model

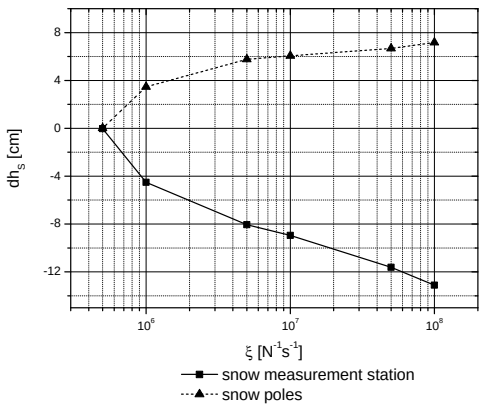

Figure 4: dh_S for different values of ξ. $F_C = 0$ N, $\rho_P = 500$ kg/m^3, $d = 500$ μm.

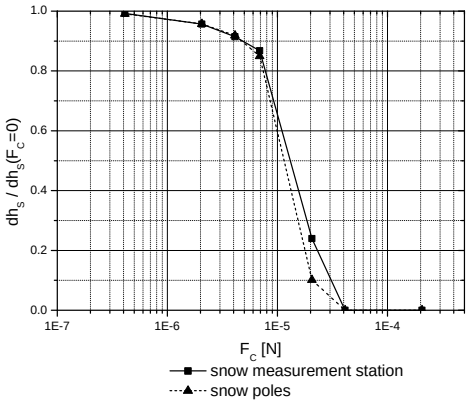

Figure 5: Ratio of dh_S to $dh_S(F_C = 0)$ for different values of F_C. $\xi = 10^6$ N^{-1}s^{-1}, $\rho_P = 500$ kg/m^3, $d = 500$ μm.

(DEM) dataset. In order to compute the snow drift and an higher resolved wind field around the snow reference station, the resolved wind field is interpolated to a smaller domain around this station. The BCs for the smaller domain are taken from the solution of the wind field simulation.

3.3 Influence of different snow property parameters

In this section the dependency on various snow property parameters of ξ, F_C, ρ_P, d (cf. Section 2.2) is analyzed. The flow field of t = 4 h is used to drive our snow drift model. The following results are achieved by a 1 h snow drift simulation. For a validation of the drift scenario see Section 3.4.

Figure 4 and 5 show a difference of the snow depth (dh_S) for different values of ξ and F_C (cf. Equation 4 and 2). The result in Figure 4 is in better agreement with the measurement for values of ξ greater than 10^6 N^{-1} s^{-1}. For $\xi = 10^5$ N^{-1} s^{-1} as proposed by Anderson and Haff (1991) no snow drift is computed. If we multiply $\xi = 10^6$ N^{-1} s^{-1} by a factor 100, dh_S will change approx. by a factor 2 to 3.

The ratio $dh_S(F_C)$ to $dh_S(F_C = 0)$ decreases approx. 15 % between $F_C = 4 \times 10^{-7}$ N and $F_C = 7 \times 10^{-6}$ N as shown in Figure 5. For higher values of F_C nearly no snow drift at the reference station occurs, because τ_t exceeds the exerted shear stress.

The particle density and diameter influences the aerodynamic entrainment of snow grains as well as deposition patterns. The grain diameter hardly depends on temperature and varies from 50 μm for rather rounded particles at low temperatures to more than 1 mm for dendrites around 0 $^\circ C$. In Figure 6 the sensitivity of dh_S for different particle diameters is computed. For an increasing diameter dh_S approaches a constant value. The increase of dh_S relative to the result for $d = 500$ μm is lower than a factor 3 for $d = 2000$ μm. dh_S decreases for approx. 70 % compared to $dh_S(d = 300$ μm$)$. It must be noted at this point, that the lower range of the particle diameter is limited by the Bagnold criteria, which are not valid for too small particles (cf. Bagnold, 1941).

For the results shown in Figure 7, we assume a packing ratio of 0.21, which determines the proportionality of snow bulk to snow particle density. The results for various particle densities are within a small range of less than $\pm$ 50 % relative to $dh_S(\rho_P = 500$ kg/m$^3)$.

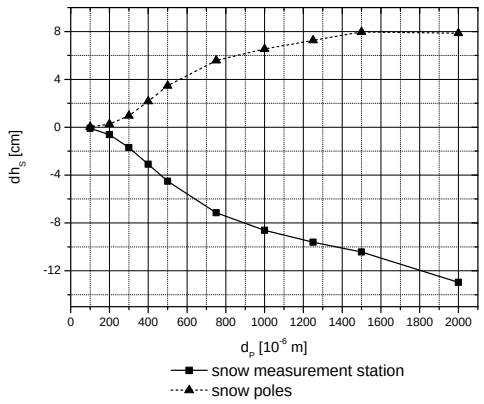

Figure 6: dh_S for different values of d. $\xi = 10^6\ \mathrm{N^{-1}s^{-1}}, \rho_P = 500\ \mathrm{kg/m^3}, F_C = 0\ \mathrm{N}$.

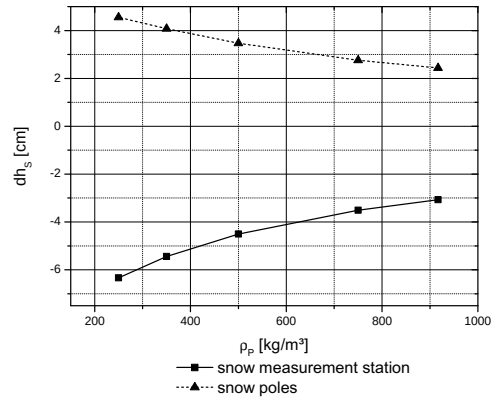

Figure 7: dh_S for different values of ρ_P. $\xi = 10^6\ \mathrm{N^{-1}s^{-1}}, F_C = 0\ \mathrm{N}, d = 500\ \mu m$.

3.4 Validation of the snow drift scenario at the 3^{rd} of March 2010

To validate the results, the snow depth is measured at the snow reference station and pictures of snow poles east of this station at a distance of 10 m are made every 2 hours. The snow reference station is located on a small ridge in downhill direction, which is touched by a chute on the east side. The automatic Ultrasonic snow depth sensor USH-8 with a resolution of 1 mm and an accuracy of 0.1 % (FS) measures the snow depth every 10 seconds and returns the 10 minute average. The snow depth at the snow poles is taken from webcam pictures with an accuracy of $\pm$ 3 cm.

Until 10^{00} CET (t=4 h) the snow depth at the station was increasing due to precipitation. Afterwards the snow depth decreased at the station because of snow drift within something less than 1 hour. The observed decrease of 7 cm is in good agreement with the simulation result, which is 8 cm in 1 hour (cf. Figure 8). For computation, the cohesion force is neglected, which is assumable at an air temperature of -7 $^\circ$C and fresh powder snow (cf. Schmidt, 1980).

Figure 9 shows the computed drift distribution, which is in good agreement with experts experiences of this area. The snow poles cannot be quantitative analyzed, because of the 2 hours time difference. But it it can be said, that the simulation reflects the tendency of the snow depth progress within the drift period.

4 CONCLUSION AND OUTLOOK

It has been shown, that the determination of time dependent boundary conditions from macro- and meso-scale NWP models by optimization techniques for micro-scale alpine wind field computations can be a good base for snow drift simulations. The result of the snow drift simulation fit the measured data in an acceptable way and the snow distribution is in good agreement with expert experi-

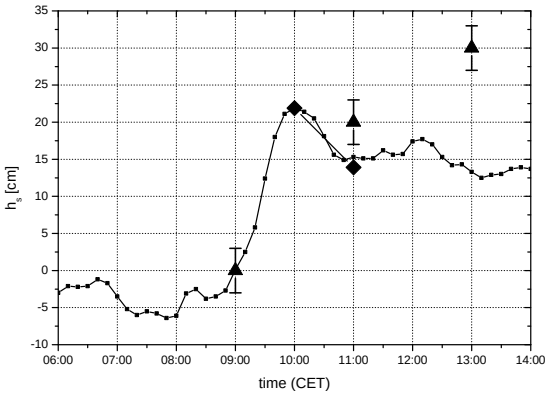

Figure 8: Progress of the relative snow depth at the snow reference station (aligned squares) compared to the 1 hour simulation result (diamond symbols). The triangles show the relative snow depth at the snow poles.

ences of this area.

Pomeroy and Gray (1990) cited a quadratic dependency of the saltation-transport rate to the friction velocity. If we compare the result for different parameters of ξ in Figure 4, we will find a logarithmical relation. Snow drift at the reference station occurs only for ξ greater than 10^6 $\mathrm{N^{-1}s^{-1}}$ and an increase of this value to 10^7 $\mathrm{N^{-1}s^{-1}}$ doubles the erosion at the weather station. In contrast a modification of the friction velocity by a factor 2 leads to a change of the snow particle flux rate by a factor 4. Compared to the driving wind speed, the results in Section 3.3 show a weaker dependency for snow property parameters. Hence, the snow drift simulation is more sensible to various wind conditions than to typical snow properties and therefore an accurate wind field is inevitable.

Nevertheless, these parameters play an important part and additional work has to be done on the huge effect of the metamorphosis of snow. Until now, no satisfactorily way of computing snow drift during precipitation is achieved, which is most important for the accumulation of snow in leeward slopes.

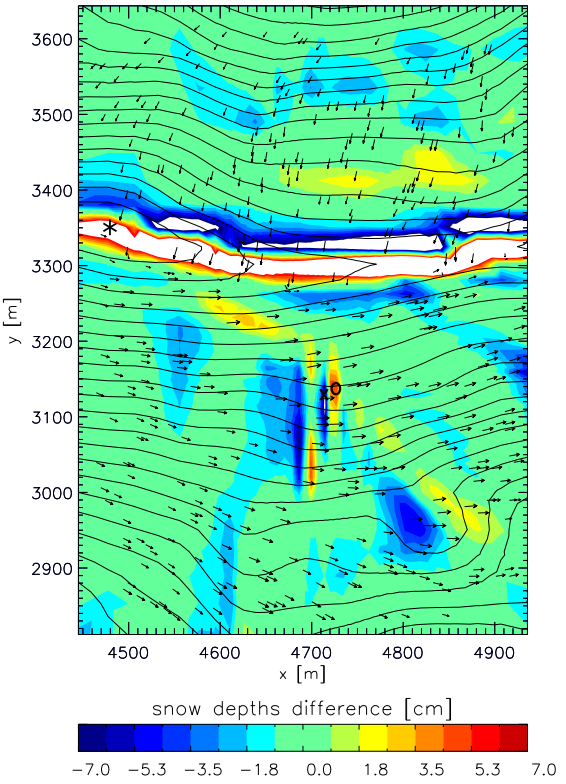

Figure 9: Snow drift simulation between 10^{00} CET and 11^{00} CET. The displayed range of the snow height is scaled from -7 cm to +7 cm and values, which are out of range are shown as white areas. Applied snow property parameters are $\xi = 5 \times 10^6$ $\mathrm{N^{-1}s^{-1}}$, $F_C = 0$ N, $d = 500$ μm $\rho_P = 500$ $\mathrm{kg/m^3}$. The length of the wind vectors correlates with the wind speed 5 m above the surface. X indicates the position of the snow reference station and O the position of the snow poles. $\star$ indicates the weather station at the Gstemmer peak. The contour lines illustrate a distance interval in z-direction of 15 m.

References

Anderson, R. and Haff, P. (1991). Wind modification and bed response during saltation of sand in air. *Acta Mechanica (Supplementum)*, 1:21–51.

Andreotti, B. (2004). A two-species model of aeolian sand transport. *Journal of Fluid Mechanics*, 510(1):47–70.

Bagnold, R. (1941). *The physics of blown sand and desert dunes*. Methuen and Co, London.

Doorschot, J. and Lehning, M. (2002). Equilibrium Saltation: Mass Fluxes, Aerodynamic Entrainment and Dependence on Grain Properties. *Boundary-Layer Meteorology*, 104(1):111–130.

Gauer, P. (1999). Blowing and Drifting Snow in Alpine Terrain: A Physically Based Numerical Model and Related Field Measurements. *Mitt. Eidgenöss. Institut für Schnee- und Lawinenforschung*, 58:128.

Lehning, M., Doorschot, J., and Bartelt, P. (2000). A snowdrift index based on SNOWPACK model calculations. *Annals of Glaciology*, 31(1):382–386.

Lehning, M., Völksch, I., Gustafsson, D., Nguyen, T. A., Stähli, M., and Zappa, M. (2006). ALPINE3D: a detailed model of mountain surface processes and its application to snow hydrology. *Hydrol. Process.*, 20(10):2111–2128.

Liston, G., Haehnel, R., Sturm, M., Hiemstra, C., Berezovskaya, S., and Tabler, R. (2007). Instruments and Methods Simulating complex snow distributions in windy environments using SnowTran-3D. *Journal of Glaciology*, 53(181):241–256.

Mott, R. and Lehning, M. (2009). Meteorological Modelling of Very High-Resolution Wind Fields and Snow Deposition for Mountains. *Journal of Hydrometeorology*, 11:934–949.

Naaim-Bouvet, F., Naaim, M., and Michaux, J. (2004). Fine scale snowdrift processes: major outcomes from Col du Lax Blanc and related experiments in wind-tunnel. *In Proceedings of the International Seminar on Snow and Avalanche Test Sites, 22-23 November 2001, Grenoble, France*, pages 249–303.

Pomeroy, J. and Gray, D. (1990). Saltation of snow. *Water Resour. Res.*, 26(7):1583–1594.

Schmidt, R. (1980). Threshold wind-speed and elastic impact in snow transport. *Journal of Glaciology*, 26(94):453–467.

Schneiderbauer, S. and Pirker, S. (2010). Resolving Unsteady Micro Scale Atmospheric Flows by Nesting a CFD Simulation into Wide Range Numerical Weather Prediction Models. *International Journal of Computational Fluid Dynamics*, 24(1):51–68.

Schneiderbauer, S. and Pirker, S. (2011). Determination of Open Boundary Conditions for Computational Fluid Dynamics (CFD) from Interior Observations. *Applied Mathematical Modelling*, 35(2):763–780.

Schneiderbauer, S., Tschachler, T., Fischbacher, J., Hinterberger, W., and Fischer, P. (2008). Computational fluid dynamic (CFD) simulation of snowdrift in alpine environments, including a local weather model, for operational avalanche warning. *Annals of Glaciology*, 48:150–158.

Shao, Y. and Li, A. (1999). Numerical Modelling of Saltation in the Atmospheric Surface Layer. *Boundary-Layer Meteorology*, 91(2):199–225.

Wang, Y., Haiden, T., and Kann, A. (2006). The Operational Limited Area Modelling System at ZAMG: ALADIN-AUSTRIA. *Oesterreichische Beitraege zu Meteorologie und Geophysik*, 37(4).

Williams, J., Butterfield, G., and Clark, D. (1990). Rates of aerodynamic entrainment in a developing boundary layer. *Sedimentology*, 37(6):1039–1048.